

Scaling laws for liftoff velocity for wind-transported particles during particle-bed collisions

ChanWen JIANG¹, Zhengcai Zhang², Zhibao Dong³, Xiaoyan Wang⁴, and Fengjun Xiao⁵

¹Weinan Normal University

²Northwest Institute of Eco-environment and Resources, Key Laboratory of Desert and Desertification, Chinese Academy of Sciences

³School of Geography and Tourism, Shaanxi Normal University

⁴College of Agricultural Business, Weinan Normal University

⁵Shaanxi Normal University

December 20, 2022

Abstract

We performed wind tunnel studies of sand-bed collisions with natural sand particles and found an impact angle of 10.5o over a loose bed, and calculated the critical impact velocity (v_{ic} [?] 1.2027 m s-1). The number of splashing particles (N_s) increased linearly with v_i , but the coefficient of restitution CoR decreased linearly with v_i . The momentum lost through frictional processes α_{lost} was insensitive to v_i , with a value of 0.2466. The mean splash velocity increased with v_i for $v_i < 7$ m s-1, and gradually reached its maximum value (0.7534 m s-1) at $v_i = 7$ m s-1, whereas decreased slowly with v_i for $v_i > 7$ m s-1 and gradually approached a constant (0.6137 m s-1). In addition, we developed a probability distribution model for liftoff velocity. Our results emphasize the crucial role of the impact angle and have significant consequences for modeling sand-bed collisions in a natural environment.

Hosted file

952214_0_art_file_10544606_rn1637.docx available at <https://authorea.com/users/567863/articles/613987-scaling-laws-for-liftoff-velocity-for-wind-transported-particles-during-particle-bed-collisions>

50 flow during a collision is negligible (Haff & Anderson, 1988, 1991). Many scholars
51 have obtained splash functions by conducting particle–bed collision experiments
52 without wind by using devices to launch the particles (Rioual et al., 2000, 2003;
53 Beladjine et al., 2007; Chen et al., 2019; Zhang et al., 2022). The most typical launch
54 devices are launch guns and centrifugal launchers. However, launch guns can only
55 launch materials with a larger than natural particle size ($d > 4$ mm) that substitute for
56 much smaller natural particles, and the airflow generated in the gun barrel would alter
57 the characteristics of the impact when they use this device to launch natural sand
58 particles ($d \cong 0.25$ mm) (Mitha et al., 1986; Rioual et al., 2000, 2003; Beladjine et al.,
59 2007). Because the splash functions are very sensitive to the density and Young's
60 modulus (deformability) of the material, launch gun experiments cannot reflect the
61 characteristics of natural sand transport well. Although centrifugal launchers can
62 launch natural sand particles without generating a disruptive airflow, it is difficult to
63 achieve an impact angle below 20° , which is much greater than the actual angle
64 during natural sand transport (Chen et al., 2019; Zhang et al., 2022). Because splash
65 functions are very sensitive to the impact angle, the resulting data don't reflect natural
66 impact processes. Therefore, it is difficult to obtain accurate splash functions for
67 natural sand with a more realistic impact angle of about 10° based on experiments
68 with too-large particles and without wind.

69

70 In this letter, we describe experimental evidence obtained through careful wind tunnel
71 measurements of collisions between saltating particles and a loose bed of natural sand.
72 We calculated the critical impact velocity ($v_{ic} \cong 1.2027 \pm 0.0791$ m s⁻¹) for aeolian
73 sand flow in air for the first time at an impact angle of 10° , and found that the splash
74 functions for sand particles with this impact angle differ quantitatively from those in
75 previous research obtained using substitute materials with a larger particle size or
76 natural sand with a larger impact angle (Beladjine et al., 2007; Chen et al., 2019).
77 However, our results support the conclusion of Ho et al. (2011) that increasing v_i will
78 lead to more splashing of particles and have less impact on the liftoff velocity (v_L).
79 Using our results, we developed a more realistic probability distribution model for v_L
80 based on the distributions of v_r and v_s . Our results emphasize the critical role of the
81 impact angle in the interactions between saltating aeolian sand particles and an
82 erodible bed.

83

84 **2. Wind tunnel experiment**

85

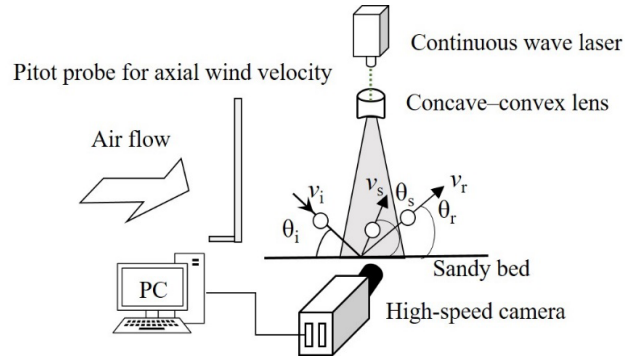
86 Our experiment was conducted in the wind tunnel of the Northwest Institute of
87 Eco-Environment Resources, Chinese Academy of Sciences, which has a total length
88 of 10.5 m and a range of axial wind speeds from 1.0 m s⁻¹ to 35.0 m s⁻¹ (Jiang et al.,
89 2022). The test section (4 m long, 0.4 m tall, and 0.4 m wide) was covered by a
90 1-cm-thick sample of dry natural sand with a range of grain sizes (hereafter, sand
91 sample G₁). Before each trial, it was gently leveled with a wooden ruler. The
92 experimental sand samples and corresponding wind conditions are shown in Table 1.
93 We recorded a total of 749 particle–bed collision events and divided them into five
94 grades according to the number of splashed particles ($N_s = 0, 1, 2, 3, \text{ or } 4$) by a
95 high-speed camera with a Micro lens (see Fig. 1). The corresponding numbers of
96 collision events were 596, 121, 24, 6, and 2, respectively. Relevant parameters during
97 collision events (i.e., the angles and velocities of impact particles, rebounding

110 particles, and splashing particles) were determined by means of particle-tracking
 111 velocimetry (Jiang et al., 2022). The average impact angle during the 749 collision
 112 events was 10.5° and the standard deviation was 4.5° . Their incidence velocity (v_i)
 113 ranged from 0.5 to 5.0 m s^{-1} .

114 **Table 1** Experimental conditions: d is the particle diameter. u^* is the wind shear
 115 velocity. G_1 was a natural desert sand from Tengger Desert in northern China, and G_2
 116 to G_7 were artificial quartz sands with good roundness (glass microbeads), which had
 117 a basic density ($\rho \cong 2650 \text{ kg m}^{-3}$) similar to that of the typical natural sand (Bagnold,
 118 1941). h , $v_{ic} / [gd]^{0.5}$, and v_{ic}/u^* are the regression parameters in equation 1 for the seven
 119 sand samples. All regressions were significant at $P < 0.05$.

Sample	d (mm)	u^* (m s^{-1})	h	v_{ic}	$v_{ic}/ [gd]^{0.5}$	v_{ic}/u^*	R^2
G_1	0.10–0.12	0.25	1.4568	1.2348	37.6088	4.9392	0.9959
G_2	0.1–0.2	0.26	1.5039	1.2421	32.3692	4.7773	0.9956
G_3	0.2–0.3	0.28	1.4461	1.1270	22.7683	4.0249	0.9769
G_4	0.3–0.4	0.31	1.6807	1.0736	18.3307	3.4631	0.9710
G_5	0.4–0.5	0.33	1.4912	1.2151	18.2969	3.6820	0.8854
G_6	0.6–0.7	0.45	1.5602	1.2125	15.1912	2.6943	0.8702
G_7	0.7–0.8	0.49	1.1968	1.3136	15.3223	2.6809	0.9916

110



111

112

113 **Figure 1.** Experimental layout and definition of the measured collision parameters. v_i
 114 and θ_i are the velocity and angle of the incident particles, respectively. v_r and θ_r are the
 115 velocity and angle of the rebounding particles, respectively. v_s and θ_s are the velocity
 116 and angle of the splashing particles, respectively.

117

118

119

3. Results

120

121

3.1. Number of splashed particles

122

123 N_s increased linearly with increasing v_i (Fig. 2A), and satisfied the equation form
 124 proposed by Beladjine et al. (2007):

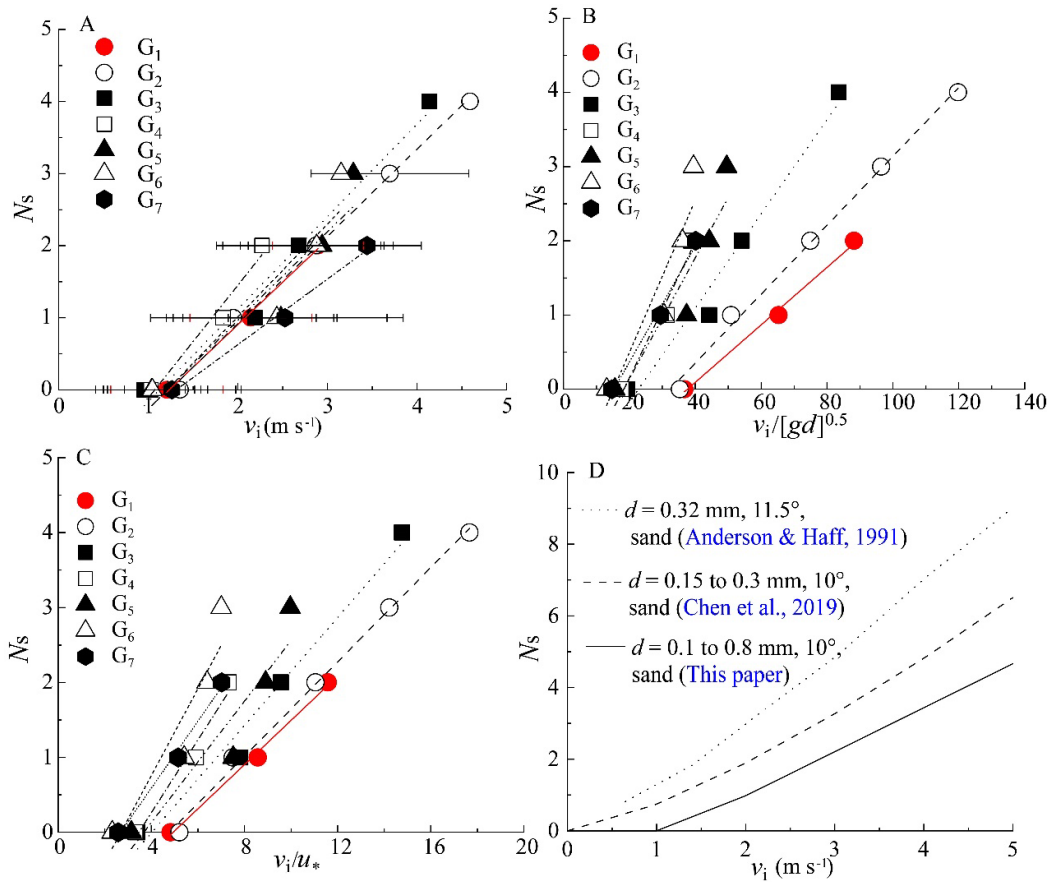
125

$$N_s = h \left(\frac{v_i}{v_{ic}} - 1 \right) \quad (1)$$

126

where h is a function of the impact angle, v_i is the impact velocity (m s^{-1}), and v_{ic} is

127 the critical impact velocity (m s^{-1}) at which splashing begins (Beladjine et al., 2007).
 128
 129



130
 131 **Figure 2.** Relationship between the number of splashed particles (N_s) and the impact
 132 velocity (v_i) (A) and v_i standardized with respect to particle size ($v_i/[gd]^{0.5}$) (B) and v_i
 133 standardized with respect to the shear velocity (v_i/u_*) (C). **Table 1** contains the
 134 regression parameters (h , $v_{ic}/[gd]^{0.5}$, and v_{ic}/u_* in equation 1) for the seven sand
 135 samples. (D) Relationship between N_s and v_i in the present study and two previous
 136 studies.

137

138 To the best of our knowledge, v_{ic} has been ignored by researchers (Anderson & Haff,
 139 1991; Chen et al., 2019). This has made it difficult to determine the critical v_L for sand
 140 particles based on their liftoff height in collision experiments without a wind
 141 (Beladjine et al., 2007). Based on the data in **Figure 2A**, we calculated v_{ic} for aeolian
 142 sand flow in air for the first time, and found that $v_{ic} \cong 1.2027 \pm 0.0791 \text{ m s}^{-1}$, as shown
 143 in **Table 1** with h at an impact angle of $10^\circ = 1.4765 \pm 0.1468$. The absolute incident
 144 velocity graphs (**Fig. 2A**) collapse well, while a comparable data collapse could not be
 145 obtained for the rescaled distributions (**Fig. 2B** and **Fig. 2C**). Thus, N_s appears to be
 146 relatively independent of the particle size (d) and wind strength (u_*).

147

148 Our results are obviously lower than the results of Chen et al.'s (2019) centrifugal
 149 particle launcher experiment and those in Anderson & Haff's (1991) theoretical
 150 model (**Fig. 2D**). The impact angles reported by Chen et al. (2019) ranged from 20° to
 151 48° ; the dashed curve in **Figure 2D** results from substituting the impact angle θ_i into

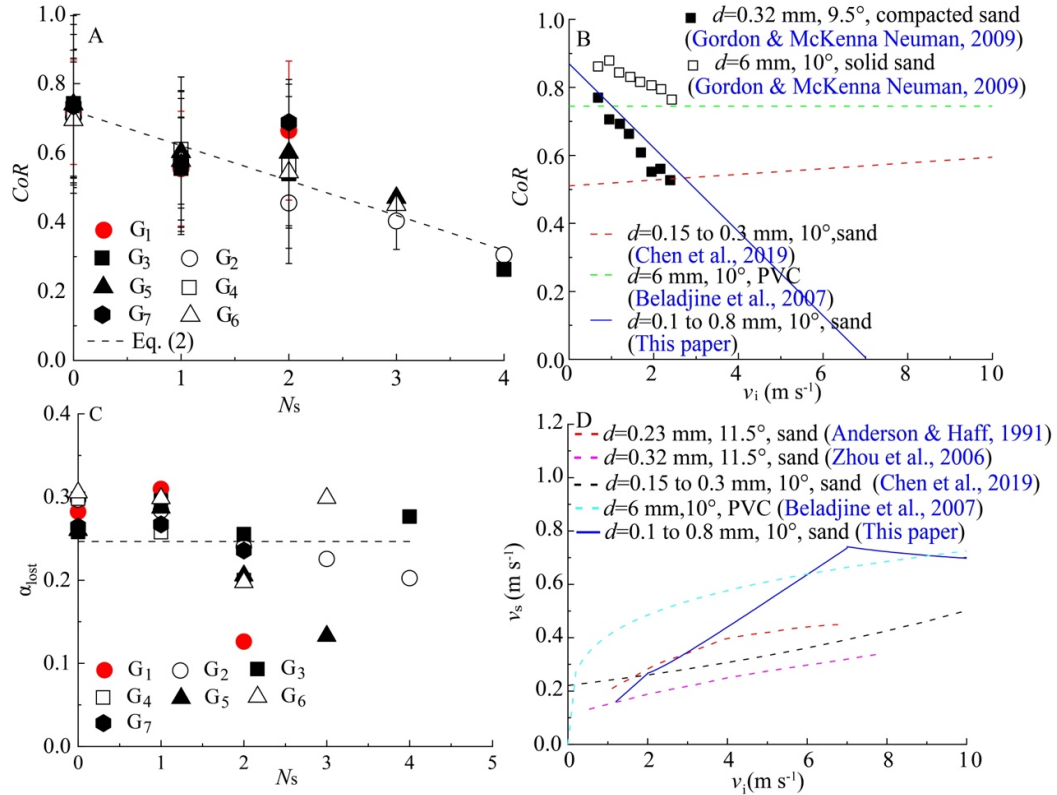
152 equation 9 in [Chen et al. \(2019\)](#). The relationship between N_s and v_i also differed
 153 greatly from that in studies that used large particles as substitute materials, such as
 154 [Beladjine et al. \(2007\)](#), who used PVC beads ($d = 6$ mm) and obtained h (at 10°) \cong
 155 5.4 and found that $v_{ic} \cong 9.7$ m s $^{-1}$ for $\theta_i = 10^\circ$.

157 3.2. Coefficient of restitution and Splash velocity

158
 159 The coefficient of restitution, $CoR = v_r / v_i$, represents the proportion of the
 160 momentum of the saltating particle that is retained when it rebounds ([Zhang et al.,](#)
 161 [2022](#)). CoR decreased linearly with increasing N_s ([Fig. 3A](#)). The equation for the
 162 probability distribution of rebound velocity proposed by [Anderson & Haff \(1991\)](#) was
 163 $P_r = 0.95(1 - \exp[-\gamma v_i])$, where P_r is the rebound probability and $\gamma = 2$ m s $^{-1}$, and
 164 mainly suggests the probability that particles with a low momentum ($v_i < 2$ m s $^{-1}$) are
 165 unlikely to rebound after a collision. In the present study, our impact velocities
 166 reached about 5 m s $^{-1}$, and if we extrapolate the graph to $N_s = 7$, we find that $CoR \cong 0$,
 167 which suggests that the impacting particles will be completely captured by the loose
 168 bed surface if $v_i > 7$ m s $^{-1}$. We can express this relationship as follows:

$$170 \quad CoR = \begin{cases} -0.1006N_s + 0.7212, & N_s \leq 7 \\ 0, & N_s > 7 \end{cases} \quad (2)$$

171



172

173 **Figure 3.** Relationships between the coefficient of restitution (CoR) and the (A)
 174 number of splashed particles (N_s) and (B) impact velocity (v_i). (C) Relationship
 175 between the frictional momentum loss fraction (α_{lost}) and the number of splashed
 176 particles (N_s). (D) The relationship between the splash velocity (v_s) and the incidence
 177 velocity (v_i).

178

179 By combining equations 1 and 2, we can obtain the relationship between CoR and v_i :

180

181

$$CoR \cong \begin{cases} -0.1235v_i + 0.8697, & v_i \leq 7.0 \text{ m/s} \\ 0, & v_i > 7.0 \text{ m/s} \end{cases} \quad (3)$$

182

183 The relationship between CoR and v_i is highly controversial. Beladjine et al. (2007)
 184 studied this relationship using PVC particles ($d = 6 \text{ mm}$) and found (Fig. 3B, green
 185 dotted line) that CoR was independent of v_i and negatively correlated with the sine of
 186 the impact angle ($CoR \cong 0.87 - 0.72 \sin \theta_i$, with θ_i expressed in radians). In contrast,
 187 Gordon & McKenna Neuman's (2009) wind tunnel results with a loose bed showed
 188 that CoR decreased linearly with increasing v_i (Fig. 3B, black solid squares).
 189 Experimental results with 5.9-mm plastic beads (Rioual et al., 2000) showed that CoR
 190 decreased slightly with increasing v_i . Chen et al. (2019) extrapolated their results from
 191 a large angle (20° to 48°) in an experiment without wind, and found that CoR
 192 increased linearly with increasing v_i when $\theta_i = 10^\circ$ and proposed that Gordon &
 193 McKenna Neuman's (2009) results may represent a special case under the condition
 194 of low v_i . However, our impact velocity reached about 5 m s^{-1} and our equation 3
 195 described Gordon & McKenna Neuman's (2009) wind tunnel results well for a loose
 196 bed (Fig. 3B, blue solid line). These results suggest that CoR is sensitive to θ_i , particle
 197 density, Young's modulus for the material, and particle size. The grain size range ($d =$
 198 0.1 to 0.8 mm) in our experiment covers most of the natural range of sand grain sizes
 199 and we found that CoR was insensitive to particle size and wind strength in this range
 200 (Fig. 3A). The basic density of the artificial quartz grains that we selected was close
 201 to that of natural sand, and Figure 3A also shows that the CoR results for natural sand
 202 with $d = 0.10$ to 0.12 mm were close to those with the artificial quartz particles of the
 203 same size. Thus, our experimental results were able to reflect the characteristics of
 204 natural sand.

205

206 According to our assumption of conservation of momentum in the collision process,
 207 the proportion of the momentum transferred to the splashed particles (α_s) can be
 208 expressed as:

209

$$\alpha_s = \frac{N_s \bar{v}_s}{v_i} = 1 - \alpha_{\text{lost}} - CoR \quad (4)$$

210

where $\alpha_{\text{lost}} = \frac{v_i - N_s \bar{v}_s - v_r}{v_i}$, and α_{lost} represents the momentum loss through frictional
 211 processes (Kok & Renno, 2009). \bar{v}_s is the mean splash speed. α_{lost} ranges between
 212 0.1 and 0.3 (Fig. 3C), and it was insensitive to N_s . This means that $\alpha_{\text{lost}} = 0.2466 \pm$
 213 0.0351 .

214

215 The expression for the mean splash velocity (\bar{v}_s) can be obtained by substituting α_{lost}
 216 into equation Eq. (4):

217

$$\bar{v}_s \cong \left(\frac{0.7534 - CoR}{N_s} \right) v_i \quad (5)$$

218

219 Based on equation (3), when $v_i > 7.0 \text{ m s}^{-1}$, $CoR = 0$. Thus, $\bar{v}_s \cong 0.7534v_i/N_s$ when
 220 $v_i > 7.0 \text{ m s}^{-1}$. Moreover, \bar{v}_s is only a realistic value if $N_s \geq 1$. Then, according to
 221 equation (1), if we assume that $N_s = 1$ and $1.2 < v_i < 2.0 \text{ m s}^{-1}$, $\bar{v}_s \cong 0.1328v_i$ based
 222 on equations (2) and (5). Therefore, if we combine equations (1), (2), (3), and (5), the
 223 relationship between \bar{v}_s and v_i can be expressed as follows:

224

$$\bar{v}_s \approx \begin{cases} 0.1328v_i & 1.2 \text{ m s}^{-1} < v_i < 2.0 \text{ m s}^{-1} \\ \frac{0.1235v_i^2 - 0.1163v_i}{1.2277v_i - 1.4765} & 2.0 \text{ m s}^{-1} \leq v_i \leq 7.0 \text{ m s}^{-1} \\ \frac{0.7534v_i}{1.2277v_i - 1.4765} & v_i > 7.0 \text{ m s}^{-1} \end{cases} \quad (6)$$

226 In addition, $\lim_{v_i \rightarrow \infty} \frac{0.7534v_i}{1.2277v_i - 1.4765} = 0.6137 \text{ m s}^{-1}$.

227

228 Equation (6) shows that when $v_i < 7.0 \text{ m s}^{-1}$, \bar{v}_s increases with increasing v_i , and the
 229 maximum splash velocity $\bar{v}_{s,\text{max}} \cong 0.7534 \text{ m s}^{-1}$ when $v_i \cong 7.0 \text{ m s}^{-1}$. In contrast,
 230 when $v_i > 7.0 \text{ m s}^{-1}$, \bar{v}_s decreases with increasing v_i and gradually approaches a
 231 constant value of 0.6137 m s^{-1} (Fig. 3D, solid blue line).

232

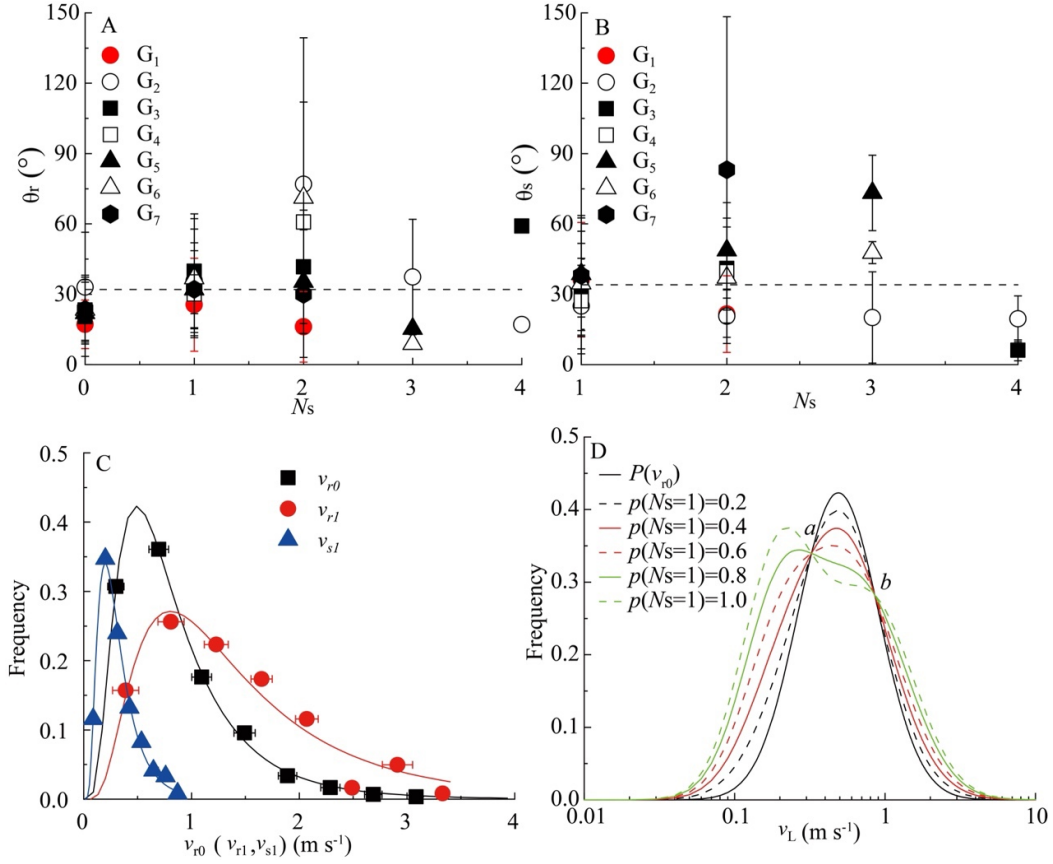
233 In our results, v_s increased with increasing v_i and there was a threshold (maximum) v_i .
 234 This agrees with the results of Beladjine et al. (2007), who proposed that v_s is
 235 proportional to the 0.25 power of v_i (Fig. 3D), and the results of Anderson & Haff
 236 (1991), who proposed that v_s was proportional to the 0.30 power of v_i (Fig. 3D).
 237 However, our results differed from the model results of Zhou et al. (2006) (Fig. 3D)
 238 and the extrapolation result of Chen et al.'s (2019) windless experiment (Fig. 3D),
 239 which showed no obvious maximum boundaries, which is quite different from our
 240 results. Equations (1), (2) and (6) support the conclusion of Ho et al. (2011) that
 241 increasing v_i will lead to more splashing of particles and have less impact on the
 242 liftoff velocity (v_L).

243

244 3.3. Probability distribution model of liftoff speed

245

246 The relationship between N_s and rebound angle (or splash angle) is not obvious (Fig.
 247 4A and 4B). However, we can roughly estimate that the mean rebound angle was
 248 $\bar{\theta}_r \cong 32 \pm 11^\circ$, and the mean splash angle was $\bar{\theta}_s \cong 34^\circ \pm 15^\circ$. Our rebound angles
 249 θ_r were similar to some previous results (Anderson & Haff's ,1991; Chen et al.,
 250 2019; Zhou et al., 2006; Xie, 2005). Therefore, when $\theta_i = 10^\circ$, θ_r may be insensitive to
 251 the particle basic density, Young's modulus of the material, and v_i . However, our
 252 splash angles θ_s were lower than most previous windless results (Chen et al., 2019;
 253 Beladjine et al., 2007; Kok & Renno, 2009). We hypothesize that a major reason for
 254 the lower θ_s in our results is that the particles that lifted off at a large angle would
 255 have been quickly diverted by the airflow.



256
 257 **Figure 4.** The relationships between the number of splashed particles (N_s) and (A) the
 258 rebound angle (θ_r) and (B) the splash angle (θ_s). Probability distributions of (C)
 259 rebound speed (v_r) and splash speed (v_s) for a number of splashed particles (N_s) of 0
 260 and 1 during collision events and (D) liftoff velocity (v_L).
 261
 262

263 The present study showed that the liftoff of particles during a steady-state sand flow
 264 are mainly composed of rebounding and splashing particles provided by collision
 265 processes. Collisions with N_s values of 0 or 1 dominated the collision events. Thus,
 266 the probability distribution function for liftoff velocity, $P(v_L)$ can be expressed as
 267 follows:

$$P(v_L) = P(v_{s1})p(N_s = 1) + P(v_{r1})p(N_s = 1) + [1 - p(N_s = 1)]P(v_{r0}) \quad (7)$$

268 where $p(N_s) = 1$ is the occurrence probability of $N_s = 1$ collision event. $P(v_{s1})$, $P(v_{r1})$,
 269 and $P(v_{r0})$ are probability distribution functions for v_s of a collision event with $N_s = 1$,
 270 for v_r of a collision event with $N_s = 1$, and for v_r of a collision event with $N_s = 0$,
 271 respectively.
 272

273
 274 By combining data from the seven sand samples described in Table 1, we obtained
 275 relatively smooth probability distribution curves for rebound velocity and splash
 276 velocity. Both v_r and v_s were described by a log-normal distribution function (see Fig.
 277 4C):

$$P(x) = A_0 \frac{\exp(-[\ln(x)-\lambda]^2/(2\delta^2))}{x} \quad (8)$$

278 where A_0 , λ , and δ are fitting values, whose values are listed in Table 2.
 279
 280

281
282
283
284

Table 2 Fitting parameters for equation 8 for the number of splashed particles (N_s) of 0 and 1 for rebound velocity (v_{r0} and v_{r1} , respectively) and for splash velocity (v_{s1}). Graphs of the distributions are shown in **Figure 4C**.

<i>Variable</i>	A_0	λ	δ	R^2
v_{r0}	0.2508	-0.3310	0.6195	0.9984
v_{r1}	0.2712	0.2196	0.6618	0.9389
v_{s1}	0.0794	-1.2963	0.5648	0.9953

285
286
287
288
289
290
291
292
293
294
295

We examined the effects of setting $p(N_s = 1)$ to 0, 0.2, 0.4, 0.6, 0.8, and 1.0, respectively, to observe the change in the probability distribution curve for v_L . All curves intersect at points a and b (**Fig. 4D**), and their corresponding x values represent two solutions for the equation $P(v_{s1}) + P(v_{r1}) + P(v_{r0}) = 0$. Because the number of bins (k) in a certain liftoff speed v_L range (we take $k = 8$ for example in **Figure 4C**) affects the corresponding fitting parameter values in equation 8, the values of a and b on the x -axis are also influenced by k . However, the value of $b-a$ on the x -axis seems to be independent of k , and is roughly constant at 0.5174 m s^{-1} . In addition, we found that a was very close to \bar{v}_{s1} and b was between \bar{v}_{r0} and \bar{v}_{r1} .

296
297
298
299
300
301
302
303
304

Figure 4D show that when particle liftoff is only generated by collision events with $N_s = 0$ or 1, then as $p(N_s = 1)$ increases, the curve gradually develops a concave-up section between a and b , and the peak gradually moves to the left. When $p(N_s = 1) = 1.0$, an obvious bimodal distribution appears. The small changes of the probability distribution curve between a and b have been ignored in previous curve fitting. Therefore, the different shapes of the probability distribution curve for v_L (**White & Schulz, 1977; Dong et al., 2002; Xie & Zheng, 2003; Cheng et al., 2006; Ho et al., 2012; Jiang et al., 2022**) may only reflect a certain stage of the development of the wind-sand flow.

305
306
307

4. Conclusion

308
309
310
311

In our wind tunnel experiment, we used natural sand and artificial quartz sand ranging from 0.1 to 0.8 mm in diameter to study the effects of particle-bed collisions. We found an impact angle of $10.5 \pm 4.5^\circ$ (mean \pm SD). We found the following novel results:

312
313
314
315
316

N_s , v_r , and v_s were relatively independent of particle size and wind strength, but were sensitive to v_i . N_s increased linearly with increasing v_i , whereas CoR decreased linearly with increasing v_i , and we were able to identify a critical impact velocity required to splash particles.

317
318
319
320
321
322
323
324

The loss of momentum through frictional processes (α_{lost}) was relatively independent of v_i and remained roughly constant. Based on the assumption of conservation of momentum during collisions, we estimated a maximum value of the mean splash speed \bar{v}_s , which differed above and below a v_i of 7.0 m s^{-1} . Below this velocity, \bar{v}_s increased approximately linearly with increasing v_i until it approached this maximum value. In contrast, above this v_i value, \bar{v}_s decreased with increasing v_i and gradually became constant.

325

326 Our calculation of the probability distributions of v_L suggests that the distributions in
327 previous research may only reflect a certain stage of the wind–sand flow.

328

329

330

331 **Acknowledgments:**

332

333 We gratefully acknowledge funding from the National Natural Science Foundation of
334 China (41901012); the Open Project funding from the Key Laboratory of Desert and
335 Desertification, Chinese Academy of Sciences (KLDD-2021-005); the Scientific
336 Research Program Funded by Shaanxi Provincial Education Department (21JP040,
337 22JS017); and the China Postdoctoral Science Foundation (2019M663615). We thank
338 Eric Parteli for fruitful discussion the physics of particle collisions, and Drs. Wanyin
339 Luo, Guangqiang Qian, and Junfeng Lu from the Key Laboratory of Desert and
340 Desertification, Northwest Institute of Eco-environment and Resources, Chinese
341 Academy of Sciences, for assisting in the wind tunnel experiment.

342

343 **Data Availability Statement**

344

345 The data used in this analysis are archived at <https://doi.org/10.5281/zenodo.7451128>

346

347 **References**

348

- 349 Anderson, R. S., & Haff, P. K. (1988). Simulation of eolian saltation. *Science*,
350 241(4867), 820-823.
- 351 Anderson, R. S., & Haff, P. K. (1991). Wind modification and bed response during
352 saltation of sand in air. *Acta Mechanica*, 1, 21-51.
- 353 Bagnold, R. A. (1941). *The Physics of Blown Sand and Sand Dunes*. William Morrow,
354 New York.
- 355 Beladjine, D., Ammi, M., Oger, L., & Valance, A. (2007). Collision process between
356 an incident bead and a three-dimensional granular packing. *Physical Review E*,
357 75(6), 061305. <https://doi.org/10.1103/PhysRevE.75.061305>
- 358 Chen, Y., Zhang, J., Huang, N., & Xu, B. (2019). An experimental study on splash
359 functions of natural sand–bed collision. *Journal of Geophysical Research:*
360 *Atmospheres* 121(14), 7226-7235.
- 361 Cheng, H., Zou, X. Y. & Zhang, C. L. (2006). Probability distribution functions for
362 the initial liftoff velocities of saltating sand grains in air. *Journal of Geophysical*
363 *Research*, III, D22205.
- 364 Chepil, W. S. (1945). Dynamics of wind erosion. Nature of soil movement by wind.
365 *Soil Science*, 60, 305-320.
- 366 Dong, Z. B., Liu, X. P., Li, F., Wang, H. T., & Zhao, A. G. (2002). Impact–
367 entrainment relationship in a saltating cloud. *Earth Surface Processes and*
368 *Landforms*, 27(6), 641–658. <https://doi.org/10.1002/esp.341>
- 369 Gordon, M., & McKenna Neuman, C. (2009). A comparison of collisions of saltating
370 grains with loose and consolidated silt surfaces. *Journal of Geophysical*
371 *Research*, 114(F4), F04015.
- 372 Ho, T.D., Valance, A., Dupont, P., & Ould El Moctar, A. (2011). Scaling law in
373 aeolian sand transport. *Physical Review Letters*, 106, 094501.
- 374 Jiang, C.W., Parteli, E. J., Dong Z.B., Zhang, Z. C., Qian, G. Q., Luo, W. Y., Lu, J.F.,

375 Xiao, F. J., & Mei, F. M. (2022). Wind-tunnel experiments of aeolian sand transport
376 reveal a bimodal probability distribution function for the particle lift-off velocities.
377 *Catena*, 217, 106496

378 Kok, J. F., & Renno, N. O. (2009). A comprehensive numerical model of steady state
379 saltation (COMSALT). *Journal of Geophysical Research: Atmospheres*, 114,
380 D17204, doi:10.1029/2009JD011702.

381 Mitha, S., Tran, M. Q., Werner, B. T., & Haff, P. K. (1986). The grain-bed impact
382 process in aeolian saltation. *Acta Mechanica*, 63(1–4), 267–278.

383 McKenna Neuman, C., & Nickling, W. G. (1994). Momentum extraction with
384 saltation. Implications for experimental evaluation of wind profile parameters.
385 *Boundary-Layer Meteorology*, 68, 35–50.

386 Owen, P. R. (1964). Saltation of uniform grains in air. *Journal of Fluid Mechanics*, 20,
387 225–242.

388 Rioual, F., Valance, A., & Bideau, D. (2000). Experimental study of the collision
389 process of a grain on a two-dimensional granular bed. *Physical Review E*, 62(2),
390 2450–2459. <https://doi.org/10.1103/PhysRevE.62.2450>

391 Rioual, F., Valance, A., & Bideau, D. (2003). Collision process of a bead on a
392 two-dimensional bead packing: importance of the inter-granular contacts.
393 *Europhysics Letters*, 61(2), 194–200.

394 Ungar, J. E., & Haff, P. K. (1987). Steady state saltation in air. *Sedimentology*, 34(2),
395 289–299.

396 White, B.R., & Schulz, J.C. (1977). Magnus effect in saltation. *Journal of Fluid*
397 *Mechanics*, 81, 497–512.

398 Xie, L. (2005) Theoretical study on liftoff velocity distribution and splash of sand
399 particles based on particle-bed collision in wind-blown sand flux. Ph.D. thesis,
400 Lanzhou University. (In Chinese)

401 Xie, L., & Zheng, X.J.(2003). Distribution of initial velocity of lift-off sand particles
402 in aeolian saltation. *Journal of Desert Research*, 23, 637–641. (In Chinese)

403 Zhang, C., Huang, N., & Dun, H. C. (2022). Experimental study on sand/bed collision
404 over the Gobi surface. *Journal of Geophysical Research: Atmospheres*, 127,
405 e2021JD035766. <https://doi.org/10.1029/2021JD035766>

406 Zhou, Y. H., Li, W. Q., & Zheng, X. J. (2006). Particle dynamics method simulations
407 of stochastic collisions of sandy grain bed with mixed size in aeolian sand saltation.
408 *Journal of Geophysical Research: Atmospheres*, 111, D15108.
409 <https://doi.org/10.1029/2005JD006604>

410

411